Post-print version of:

Publisher: **Elsevier**

Journal paper: **Engineering Fracture Mechanics 2013, 98(1) 153-168**

Title: **An application of the weight function technique to inclined surface cracks under rolling contact fatigue, assessment and parametric analysis**

Authors: **M. Beghini, C. Santus**

Creative Commons Attribution Non-Commercial No Derivatives License

DOI Link: https://doi.org/10.1016/j.engfracmech.2012.10.024

An application of the weight function technique to inclined surface cracks under rolling contact fatigue, assessment and parametric analysis

M. Beghini[a], C. Santus[a*]

[a]University of Pisa. Department of Civil and Industrial Engineering. Largo L. Lazzarino 2, 56126 Pisa, Italy.

Abstract

This paper proposes the use of the weight function technique to calculate mode I and mode II stress intensity factors for a shallow surface crack typical of rolling contact fatigue, that experiences the detrimental effects of the pressurization of lubricating fluid. The weight function technique was able to easily take the pressurization into account just by adding the pressure term to the nominal stress component which is then integrated. The crack closure was also modeled by introducing an assumption for the distribution of the contact pressure on the crack face. The results were validated with the literature data and finite element analyses. Parametric simulations were performed showing that mode I and mode II stress intensity factors strongly depend on the crack angle with respect to the surface, and almost linearly on the size of the crack. In addition, the proposed algorithm was able to include any residual stress distribution. Compressive residual stress hinders pressurization and promotes the crack closure. This effect was parametrically investigated and it was found that cracks, and especially small ones, can even remain closed, with the opening effect of the pressurization completely suppressed.

Keywords:
Weight functions. Stress intensity factors. Rolling contact fatigue. Lubricating fluid pressurization.

*Corresponding author: Ciro Santus
Ph. +39 (0)50 2218007 Fax +39 (0)50 2218065
email: `ciro.santus@ing.unipi.it`

1 Introduction

Rolling Contact Fatigue (RCF) *pitting* and *micropitting* are common surface damage phenomena detected in bearings and gears [1, 2, 3, 4]. These mechanisms originate on the *surface* and are usually observed under mixed lubricating conditions with "as ground" surface finish [5, 6]. Subsurface *spalling*, on the other hand, is typically generated under very smooth (polished) contacting surfaces and good lubrication conditions [2, 3]. The initiation and propagation of pitting surface cracks are very different from spalling subsurface cracks, as they are directly exposed to surface contact and to the effects of the lubricating fluid. There are two phases in the evolution of pitting, which can be confirmed by surface observation. Initially, several shallow microcracks appear on the surface. These cracks subsequently experience "pressurization" (or "fluid pumping") which promotes their growth. The lubricating fluid fills the internal volume of the surface crack, where it is then pressurized by the passing contact load. The internal fluid pressure is assumed to be as high as the pressure due to contact, since it is in direct communication with the contact interface. Olver et al. [7] showed a typical V–shaped (or arrow head) micropit crack that was initially filled by the lubricating fluid, after which the fluid was expelled. During pressurization produced by the contact transit, the crack faces are pulled apart by the fluid pressure and the mode I Stress Intensity Factor (SIF) is positive and experiences a cycle [8]. Way [9] was the first to obtain experimental evidence that the lubricating fluid enhanced the formation of pitting damage. After his pioneering work, the pressurization mechanism was investigated, both experimentally and analytically through numerical simulations. Datsyshyn and Marchenko [10] presented a survey of different models of the pressurized surface crack problem loaded by a Hertz–like pressure distribution contact transit. In Bower's paper [11], which dealt with pressurization and entrapment phenomena, the crack SIFs were obtained by the dislocation distribution method, previously proposed by Keer and Bryant [12]. The dislocation distribution technique was also applied by Johnson [13] and, more recently, by Jin et al. [14]. Murakami et al. [15] used a Finite Element (FE) 3D model that reproduces the typical arrow head shape of the crack. Even though a plane model can not take into account the effects of the boundaries and the angle between the two fronts of the "arrow head", the shape of the pitting crack suggests the use of a plane (2D) model since the width is usually much larger than the depth. Fajdiga and Glodež et al. [3, 16, 17, 18] used plane FE models (with the virtual crack extension method) to calculate the SIFs of the fluid pressurized fatigue crack, and Ringsberg and Bergkvist [19] also used FE simulations, by implementing the quarter point method to calculate the SIFs.

This paper proposes an alternative to FE analysis in order to solve the pressurization surface crack plane problem using the Weight Function (WF) technique to calculate both mode I and mode II SIFs. In previous works Beghini et al. [20, 21, 22, 23] developed a parametric WF for a surface crack with a generic angle, the same geometry as the present problem. The partially closed crack was also considered, Beghini et al. [22], and was solved with the WF technique by introducing an extra term, on the nominal stress, equal to the contact pressure between the partially closed crack faces. Similarly, the WF approach can model the pressurization effect just by adding a positive term (equal to the fluid pressure) to the nominal stress. In addition, the WF formulation can also consider a residual stress distribution, which is typically present in components subjected to RCF. Again, a further stress term is simply added to the nominal stress before the WF integration.

This numerical technique is applied in the present paper to a classic Hertz contact pressure distribution with friction traction, traveling over the crack. The proposed algorithm can be also applied to non Hertzian contacts or distributions that change during the transit over the crack. In order to validate the proposed procedure, comparisons with other research results are reported along with numerical results obtained with a dedicated FE model.

Finally, by taking advantage of the efficiency of the WF approach, a large parametric analysis was performed and trends of the resulting SIFs are reported and discussed. The effect of the residual stress was also investigated. Obviously, a compressive residual stress state hinders the opening of the crack by reducing the range of the mode I SIF, whereas a tensile residual stress increases the mode I cycle experienced by the surface crack during the contact transit. This effect is extremely dependent on the size of the crack. The smaller the crack, the larger the closure effect, with a compressive residual stress state. A small crack can even be completely closed by compressive residual stresses, as shown in the final section of the paper. The crack needs to increase its size, by cyclic shear stress fatigue, before experiencing propagation supported by pressurization [24], hence the pitting damage is delayed or even prevented.

2 Fluid pressurization of shallow surface cracks

The formation of a pit crack has a preliminarily phase in which microcracks initiate on the surface, Fig. 1. The orientation of these microcracks is related to the sliding direction and is independent of the direction of the rolling motion. The small surface angle between the microcrack and the surface is typically in the range $20° - 30°$ [5, 8].

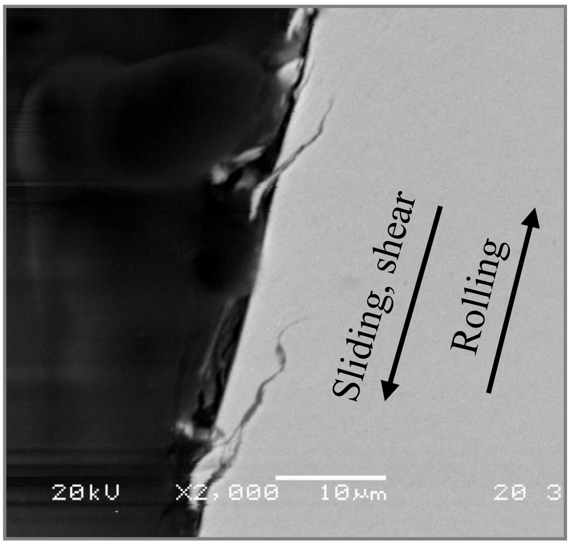

Figure 1: Shallow surface microcracks, opposite to the sliding direction (or the friction traction).

Once a surface crack has been nucleated and if the crack is kept open while the contact is approaching, the lubricating fluid fills the open volume between the crack faces. This fluid inside the crack undergoes a strong pressure increase (pressurization) while the contact region passes over the crack mouth. As a consequence the crack experience a mode I stress intensity factor transient. Pressurization is effective only if the sliding direction is opposite to the contact motion [7]. This condition is referred to as a *negative* Slide to Roll ratio ($S/R < 0$), and is experienced by the slower of the two mating surfaces [7], e.g. the *follower* in a (twin) disc experiment, Fig. 2(a), while $S/R > 0$ is experienced by the faster surface, Fig. 2(b). The intensity of the slide to roll ratio S/R is defined as the ratio between the difference of the velocities of the two mating surfaces, over the velocity of one surface compared to the contact, which is the rolling velocity [25]. Alternatively, the average velocity of the two bodies can be considered (the entrainment velocity) [7], in order to have the same S/R intensity for the two mating bodies, and only have a different sign between the follower and the driver. In this paper just the sign of the S/R ratio was considered.
Under the two conditions: negative S/R and opposite surface crack orientation to the sliding, it was hypothesized (and confirmed by experiments) that shallow cracks are kept open while the contact is approaching, thus the pressurization is active. If any of these two conditions is not satisfied, e.g. if the S/R is positive, the crack remains closed, it is not filled by the fluid and pressurization does not happen. As a consequence, more pronounced pitting is experienced by the follower surface. In gears, surface pitting is usually found on *dedendum* tooth flanks (both for driven and driver gears) where the S/R ratio is negative [7, 13, 26, 27].

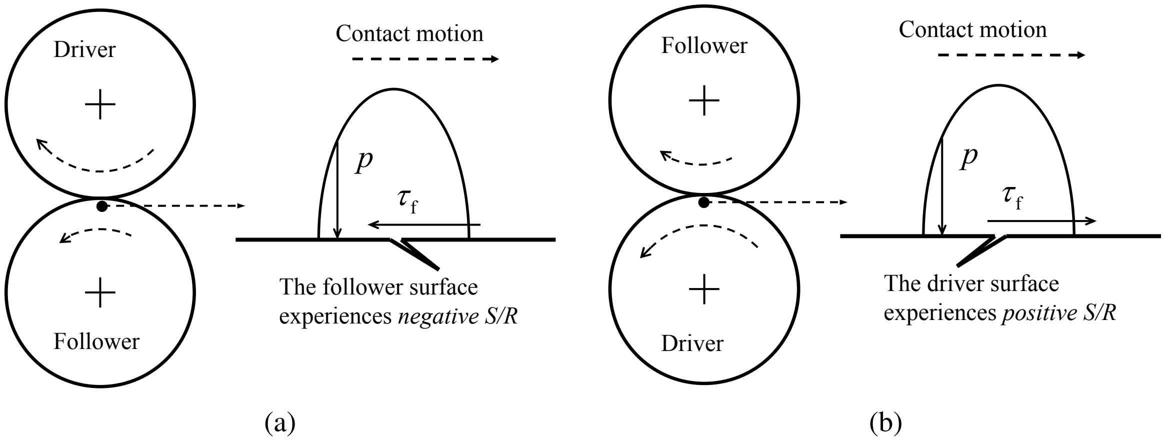

Figure 2: S/R ratio on twin disc testing: (a) follower $S/R < 0$, (b) driver $S/R > 0$.

The paper by Bower [11] widely describes the phenomenon and identified two phases: *pressurization* and the *entrapment* of the fluid inside the crack. During pressurization, the fluid inside the crack is connected with the contact region, while the entrapment is obtained afterwards, when a certain volume of fluid is stored inside the crack and the crack mouth is closed by the contact. The fluid inside the entrapment volume experiences a pressure peak, which can be even higher than the contact pressure during pressurization. Finally, the fluid is expelled when the contact transit recedes. The entrapment mechanism is possible only if the crack has a comparable size or is larger than the width of the contact region, as shown by Bower [11]. If the crack is relatively long, compared to the contact width, the crack mouth experiences a strong closing pressure, while the action is much weaker at the crack tip, thus the volume of fluid in the lower part of the crack remains isolated. On the other hand, if the crack is smaller than the contact width, the entrapment is not expected to happen being the fluid already expelled before crack closure, Fig. 3. The typical size of pitting cracks, experienced by high strength steel for bearings and gears, is usually in the order of 10^{-2} mm, Fig. 1. They are therefore quite small compared to the typical contact width that is usually in the order of 10^{-1} mm. As a consequence, the numerical analysis reported in this paper was based on the assumption of no fluid entrapment. The crack was either open (communicating with the contact pressure) or simply closed without any pressurization, and no transient was modeled between the two situations. During pressurization, the distribution on the pressurized crack faces was considered to be uniform, as usual in the literature [3, 11, 16, 17, 18]. The friction between the crack faces was neglected, and perfect lubrication was assumed. Though this hypothesis is questionable and overcome in other studies, crack face friction would introduce stick & slip on different areas along the crack length, and the partial open crack condition should be considered. The value of the coefficient of friction, between the crack faces, is impossible to measure, thus an estimated value is needed. In addition, the main detrimental effect produced by pressurization is the positive mode I transient, during which the crack faces are not in contact.

3 Weight function model

The Weight Function (WF) is a powerful computational tool used in linear elastic fracture mechanics to calculate crack Stress Intensity Factors (SIFs) and also crack opening displacement. The main assumption is that any non linear effect, such as large plasticity, is absent or negligible [28]. The SIFs are obtained by integrating, over the crack domain, the *nominal* stress distribution, multiplied by the WF as a kernel. The nominal stress distribution is the stress acting on the crack assuming an *uncracked* body (or before the crack formation), i.e. the local stress acting on the crack region. Another fundamental assumption is that the presence of the crack does not significantly modify the external load, with respect to the uncracked geometry. This assumption,

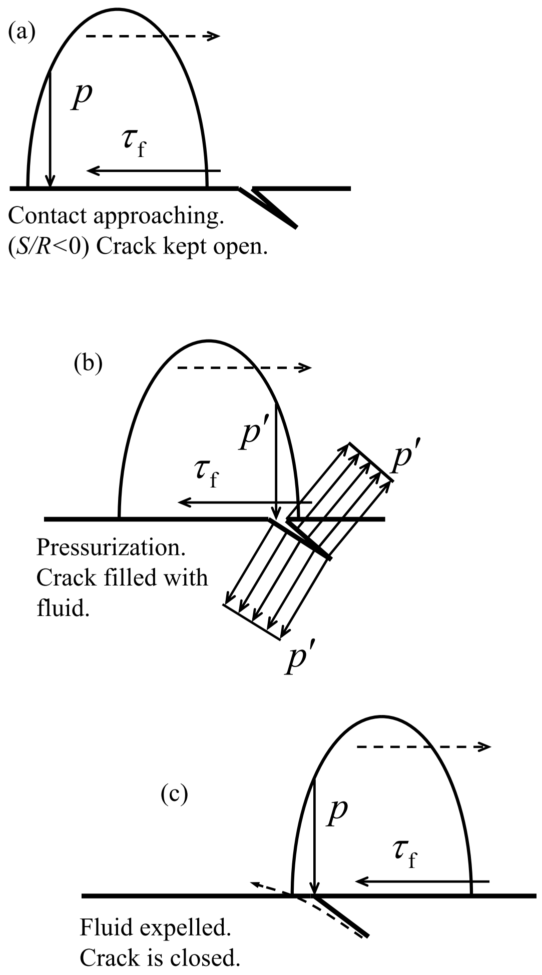

Figure 3: Steps of the lubricating fluid pressurization.

applied for the present problem, requires that the Hertz normal pressure and friction shear keep the same distributions even with the surface crack, which is reasonable when the crack is small compared to the contact area. The WF only depends on the crack geometry, and is unaffected by the nominal stress distribution. WF closed forms are known for a few simple cases, however, approximated but accurate enough expressions can be found for specific geometries. Approximate analytical expressions can be obtained by assuming a parametric general form of the WF, and by fitting the parameters with specific accurate FE solutions.

3.1 Surface inclined crack weight function

As previously mentioned, surface microcracks have a large width over depth ratio, thus they can be reasonably well modeled as straight cracks in a half–plane (2–D model), even though they show some irregularities, Fig. 1. The geometry parameters to define the crack are, therefore, the angle θ and the crack length c, Fig. 4. Beghini et al. [20, 21, 22, 23] obtained the WF for a plane surface crack, inclined of a general angle. In order to obtain the fracture parameters, the nominal stress components need to be expressed in the local coordinates x', y', Fig. 4 (a). Both the stress components $\sigma_{y'y'}, \sigma_{x'y'}$ (normal and shear) affect the two SIFs $K_{\mathrm{I}}, K_{\mathrm{II}}$, while the stress component $\sigma_{x'x'}$ and out of plane normal stress have no effect.
If the angle θ is different from $\pi/2$, the nominal normal stress $\sigma_{y'y'}$ primarily contributes to mode I SIF but also

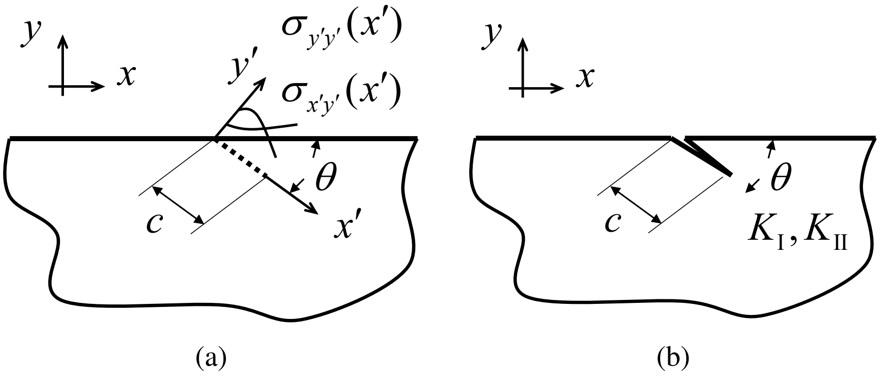

Figure 4: (a) Nominal stress distribution: the stress at the crack line, assuming uncracked body. (b) Plane model crack SIFs.

to mode II. Similarly, the nominal shear stress $\sigma_{x'y'}$ contributes more intensively to mode II, but also to mode I. The coupling effect, due to the asymmetry of the problem, can be accounted for by a matrix formulation of the WF. The integration of the WF matrix is expressed by Eq. 1.

$$\begin{bmatrix} K_\mathrm{I} \\ K_\mathrm{II} \end{bmatrix} = \int_0^c \begin{bmatrix} h_{11}(x',c,\theta) & h_{12}(x',c,\theta) \\ h_{21}(x',c,\theta) & h_{22}(x',c,\theta) \end{bmatrix} \begin{bmatrix} \sigma_{y'y'}(x') \\ \sigma_{x'y'}(x') \end{bmatrix} \mathrm{d}x' \tag{1}$$

where $x' = 0$ is the crack mouth and $x' = c$ is the crack tip position. The out of diagonal WF components $h_{12}(x',c,\theta), h_{21}(x',c,\theta)$ vanish, and the matrix integration is reduced to scalar integrations, only for $\theta = \pi/2$. The WF components $h_{hk}(x',c,\theta)$ can be accurately approximated by Eq. 2, the WF component coefficients $\alpha_i^{hk}(\theta)$ can be expressed by Eq. 3 and the dimensionless coefficients λ_{ij}^{hk} are reported in Tab. 1.

$$\begin{aligned} h_{hk}(x',c,\theta) &= \sqrt{\frac{2}{\pi c}} \left[\left(1 - \frac{x'}{c}\right)^{-1/2} + \sum_{i=1}^{4} \alpha_i^{hk}(\theta) \left(1 - \frac{x'}{c}\right)^{i-1/2} \right], \quad \text{for } hk = 11 \text{ or } hk = 22 \\ h_{hk}(x',c,\theta) &= \sqrt{\frac{2}{\pi c}} \left[\sum_{i=1}^{4} \alpha_i^{hk}(\theta) \left(1 - \frac{x'}{c}\right)^{i-1/2} \right], \quad \text{for } hk = 12 \text{ or } hk = 21 \end{aligned} \tag{2}$$

$$\begin{aligned} \alpha_i^{hk}(\theta) &= \lambda_{i1}^{hk} \tan^2(\theta - \pi/2) + \textstyle\sum_{j=2}^{5} \lambda_{ij}^{hk} \cos((j-2)(\theta - \pi/2)), \text{ for } hk = 11 \text{ or } hk = 22 \\ \alpha_i^{hk}(\theta) &= \lambda_{i1}^{hk} \tan^2(\theta - \pi/2) \sin(\theta - \pi/2) + \textstyle\sum_{j=2}^{5} \lambda_{ij}^{hk} \sin((j-1)(\theta - \pi/2)), \text{ for } hk = 12 \text{ or } hk = 21 \end{aligned} \tag{3}$$

The overall accuracy of this WF calculation is in the order of 1%, provided that the angle θ is within the range $15^\circ - 165^\circ$. This angle limitation is caused by the form of the analytical approximation, however, it does not introduce a limitation for the present problem, since the crack angle is never lower than 15°. Further details regarding the proposed WF are reported in Ref. [20].

3.2 Calculation of the SIFs both with pressurization and crack faces in contact

The weight function technique can be used to model the fluid pressurization very efficiently. When there is pressurization, the SIFs ($K_\mathrm{I}, K_\mathrm{II}$) are the result of Eq. 1 integration, where the pressure evaluated at the surface contact crack mouth position p' is added to the normal nominal stress $\sigma_{y'y'}$. In general the surface contact load produces a negative (closing) nominal stress contribution, while the fluid pressure produces a positive (opening) nominal stress contribution. Intuitively, the surface contact pressure tends to close the crack, while

λ_{ij}^{11}	$i=1$	2	3	4
$j=1$	0.352260648	0.561740777	0.002757774	−0.082522228
2	20.12858867	−6.75915207	14.69890758	−6.555566564
3	−28.35443914	12.21105233	−24.64961078	10.87434602
4	10.61781505	−6.721903843	13.14073974	−5.893279322
5	−1.794159914	1.272090422	−2.589806357	1.200996132
λ_{ij}^{12}	$i=1$	2	3	4
$j=1$	0.04401007	−0.088936286	0.09297728	−0.035669115
2	5.730314603	−11.04002435	12.13325221	−4.883436003
3	−4.413898809	10.19534617	−11.84935675	4.856493593
4	1.598258465	−3.559021699	4.07900429	−1.676244823
5	−0.257065332	0.515781329	−0.548201846	0.214198514
λ_{ij}^{21}	$i=1$	2	3	4
$j=1$	0.177883032	0.728488774	−0.248806075	0.023045677
2	0.808784091	17.6992381	−10.7581263	3.112044367
3	0.101895496	−16.00705368	11.92486888	−4.026999105
4	−0.023285672	5.675420857	−3.879295621	1.234486015
5	0.001237758	−0.851326701	0.497548624	−0.133053283
λ_{ij}^{22}	$i=1$	2	3	4
$j=1$	0.114487102	−0.22899214	0.242228468	−0.093044459
2	8.781169684	−11.51130605	11.0665334	−4.245644102
3	−12.02782951	19.63198074	−19.64671793	7.575469487
4	4.571171695	−9.876681231	11.38812338	−4.668556109
5	−0.723370423	1.708779212	−2.077090179	0.884130668

Table 1: Angle coefficients to calculate the weight function components, after Beghini et al. [20].

the fluid pressure tends to separate the crack faces. The pressurization may dominate in particular positions of the contact during the transit. Nominal stresses are not applied to the faces of the crack in the real physical problem, while pressurization is actually applied to the faces of the crack (reproducing the exact loading conditions of the weight function problem). Despite this distinction, these two contributions to the SIFs can be correctly superimposed. In addition, the superimposition can be applied to the stress components before performing the WF integral. It is also possible to take any residual stress distribution into account, which is common in bodies used for contact loads. This contribution of residual stress is added to both the nominal stress components $\sigma_{y'y'}, \sigma_{x'y'}$ which are then inputted in Eq. 1. The overall nominal stresses are given by Eq. 4.

$$\begin{aligned} \sigma_{y'y'}(x') &= \sigma_{y'y'}^{p,\tau}(x') + \sigma_{y'y'}^{\mathrm{RS}}(x') \\ \sigma_{x'y'}(x') &= \sigma_{x'y'}^{p,\tau}(x') + \sigma_{x'y'}^{\mathrm{RS}}(x') \end{aligned} \tag{4}$$

The stresses $\sigma_{y'y'}^{\mathrm{RS}}(x'), \sigma_{x'y'}^{\mathrm{RS}}(x')$ are the residual stress contributions, while $\sigma_{y'y'}^{p,\tau}(x'), \sigma_{x'y'}^{p,\tau}(x')$ are the nominal stress components produced by surface contact pressure and friction traction. These stress distributions need to be calculated from the contact pressure and friction, at different times during the contact transit. This problem can be solved numerically, by approximating the applied pressure and traction as a traveling discrete sequence of uniform distributions, Fig. 5.
The stress components at any position $A(x,y)$ below the surface can be calculated in closed form for any

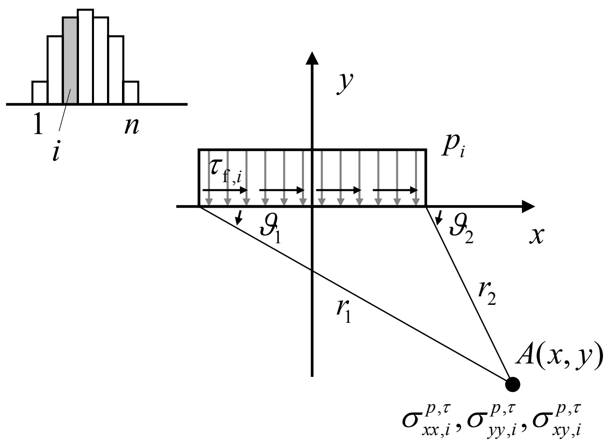

Figure 5: Stress distribution at any position below the surface, produced by uniform pressure plus uniform shear traction.

uniform distribution, Eq. 5 [29].

$$
\begin{aligned}
\sigma^{p,\tau}_{xx,i} &= -\frac{p_i}{2\pi}\left(2(\vartheta_1-\vartheta_2)+(\sin 2\vartheta_1-\sin 2\vartheta_2)\right)+\frac{\tau_{\mathrm{f},i}}{2\pi}\left(4\ln\frac{r_1}{r_2}-(\cos 2\vartheta_1-\cos 2\vartheta_2)\right)\\
\sigma^{p,\tau}_{yy,i} &= -\frac{p_i}{2\pi}\left(2(\vartheta_1-\vartheta_2)-(\sin 2\vartheta_1-\sin 2\vartheta_2)\right)+\frac{\tau_{\mathrm{f},i}}{2\pi}(\cos 2\vartheta_1-\cos 2\vartheta_2)\\
\sigma^{p,\tau}_{xy,i} &= -\frac{p_i}{2\pi}(\cos 2\vartheta_1-\cos 2\vartheta_2)+\frac{\tau_{\mathrm{f},i}}{2\pi}\left(2(\vartheta_1-\vartheta_2)+(\sin 2\vartheta_1-\sin 2\vartheta_2)\right)
\end{aligned}
\tag{5}
$$

Obviously, the stresses $\sigma^{p,\tau}_{y'y'}, \sigma^{p,\tau}_{x'y'}$ are obtained by summing up all the terms $\sigma^{p,\tau}_{xx,i}, \sigma^{p,\tau}_{yy,i}, \sigma^{p,\tau}_{xy,i}$, and then applying the (plane) tensorial rotation. Any contact pressure and friction traction distributions can be approximated as a step function with a reasonable number of divisions, and the stress components $\sigma^{p,\tau}_{xx}, \sigma^{p,\tau}_{yy}, \sigma^{p,\tau}_{xy}$ can be obtained at any point, and at any position of the traveling load, by updating the coordinates $\vartheta_1, \vartheta_2, r_1, r_2$.
The Hertz pressure distribution is defined by the half–width of contact a, the pressure distribution center position x_c and the maximum pressure value p_0. The discretization is performed by calculating the Hertz pressure value at the mid point of each i–th segment x_i:

$$
\begin{aligned}
&p_i = p_0\sqrt{1-\left(\frac{x_i-x_\mathrm{c}}{a}\right)^2}, \quad \text{if } |x_i-x_\mathrm{c}|\le a\\
&p_i = 0, \quad \text{if } |x_i-x_\mathrm{c}|> a\\
&\tau_{\mathrm{f},i} = f p_i
\end{aligned}
\tag{6}
$$

Fig. 6(a) shows a Hertz like contact distribution at different locations during the contact transit, and Fig. 6(b) shows the $\sigma^{p,\tau}_{yy}$ component calculated in a whole rectangular domain, for a given position of the traveling contact pressure and shear friction distributions, though the stresses are only required along the crack line for the WF integration.
Although this paper only considers the Hertz pressure distribution, and proportional friction, the contact distribution can be more general by following this step function discretization. For instance, the elastohydrodynamic contact distribution can also be considered [30], or any not Hertzian pressure distribution generated by discontinuous curvature contacting profiles [31].

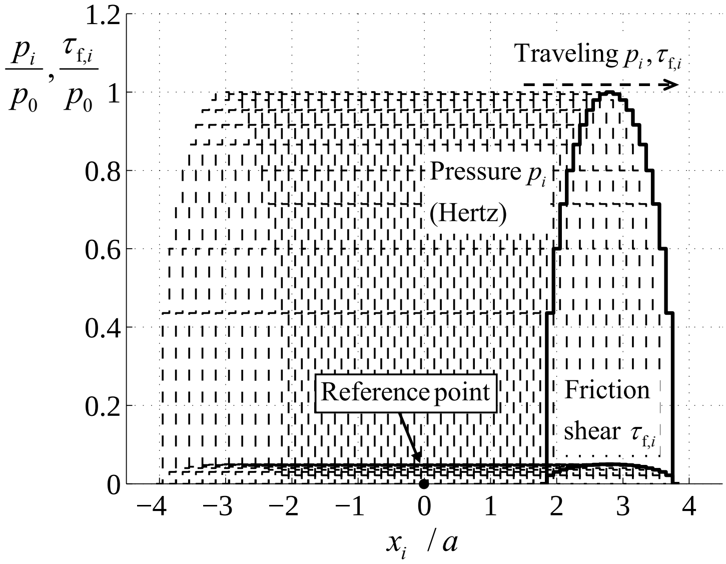

(a)

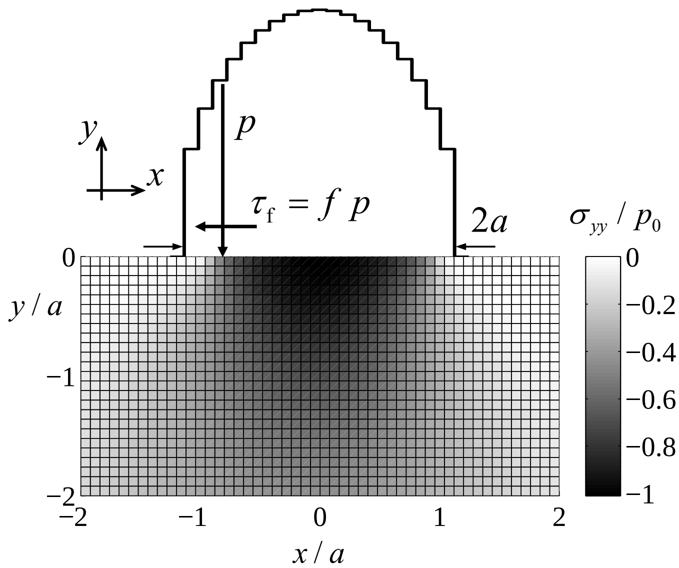

(b)

Figure 6: (a) Hertz distribution as a step function. (b) Normal stress component distribution below the surface when the pressure maximum is at the reference point.

Two different crack loading contact conditions need to be distinguished before calculating the WF integrals: pressurization, and closed crack. The pressure value p' is added to the nominal normal stress $\sigma_{y'y'}(x')$ when the crack is pressurized, Eq. 7:

$$\begin{bmatrix} K_\mathrm{I} \\ K_\mathrm{II} \end{bmatrix} = \int_0^c \begin{bmatrix} h_{11}(x',c,\theta) & h_{12}(x',c,\theta) \\ h_{21}(x',c,\theta) & h_{22}(x',c,\theta) \end{bmatrix} \begin{bmatrix} \sigma_{y'y'}(x') + p' \\ \sigma_{x'y'}(x') \end{bmatrix} \mathrm{d}x' \tag{7}$$

If the crack is closed (and as a consequence not pressurized) the first SIF is null, and the crack faces contact pressure distribution $p_\mathrm{c}(x')$ is included instead of p' to calculate the mode II SIF, Eq. 8:

$$\begin{bmatrix} 0 \\ K_\mathrm{II} \end{bmatrix} = \int_0^c \begin{bmatrix} h_{11}(x',c,\theta) & h_{12}(x',c,\theta) \\ h_{21}(x',c,\theta) & h_{22}(x',c,\theta) \end{bmatrix} \begin{bmatrix} \sigma_{y'y'}(x') + p_\mathrm{c}(x') \\ \sigma_{x'y'}(x') \end{bmatrix} \mathrm{d}x' \tag{8}$$

The integration of Eq. 7, or Eq. 8, can be solved numerically with a computer program, at any load position during the contact transit, using the proposed numerical forms of the WF components and the nominal stress calculations as described above. The two conditions, pressurization or closed crack, can be distinguished according to the following algorithm:

1. The contact transit is divided into steps. As initial step, a position which is approaching and sufficiently away from the crack mouth is assumed where pressurization does not apply, since the pressure distribution is not over the crack. The procedure is repeated for each step that the contact transit is divided into, until the contact distribution is at the other side, away from the crack mouth and its effect on SIFs is vanishingly small.

2. If $S/R < 0$ and the surface load is over the crack mouth, the pressurization is taken into account. The $K_{\mathrm{I}}, K_{\mathrm{II}}$ values are calculated by the WF integration, with the pressurization term, Eq. 7, and the contact pressure p' is evaluated at the crack mouth. If $S/R \geq 0$ or the surface load is away from the crack mouth, Eq. 7 is preliminarily used with $p' = 0$.

3. If $K_{\mathrm{I}} > 0$ no further modification is required and the obtained values $K_{\mathrm{I}}, K_{\mathrm{II}}$ are recorded for the generic i–th step. When the surface load is approaching, the crack can be open because of the friction traction and the use of Eq. 7 with $p' = 0$ (no pressurization) can give a positive, though small, K_{I} value. With negative K_{I} result, on the other hand, the introduction of a crack face contact distribution $p_{\mathrm{c}}(x')$ is required, in order to re–establish the closed crack $K_{\mathrm{I}} = 0$ condition, and a corrected value of K_{II} needs to be recalculated.

When $K_{\mathrm{I}} < 0$ has been obtained, there is no unique crack face contact pressure distribution producing null K_{I}. The correct $p_{\mathrm{c}}(x')$ pressure distribution should also satisfy the condition of zero crack opening displacement, over the entire crack. To solve the problem without iterative calculation, an assumption on the $p_{\mathrm{c}}(x')$ trend was introduced. The proposed hypothesis is that $p_{\mathrm{c}}(x')$ is proportional to the nominal stress normal component $\sigma_{y'y'}(x')$, Eq. 9:

$$p_{\mathrm{c}}(x') = \lambda_{\mathrm{c}} \sigma_{y'y'}(x') \tag{9}$$

The reason for this assumption is that the nominal normal stress distribution would produce zero SIFs and zero crack opening displacement (when acting with the nominal shear stress), thus it is assumed to be a good basis for the crack face contact distribution. After this hypothesis, the $p_{\mathrm{c}}(x')$ unknown reduces to a single scalar dimensionless factor λ_{c}. The Equation 8 can be rewritten as:

$$\begin{bmatrix} 0 \\ K'_{\mathrm{II}} \end{bmatrix} = \int_0^c \begin{bmatrix} h_{11}(x',c,\theta) & h_{12}(x',c,\theta) \\ h_{21}(x',c,\theta) & h_{22}(x',c,\theta) \end{bmatrix} \begin{bmatrix} \sigma_{y'y'}(x') + \lambda_{\mathrm{c}} \sigma_{y'y'}(x') \\ \sigma_{x'y'}(x') \end{bmatrix} \mathrm{d}x' \tag{10}$$

and λ_{c} can be found by solving the first equation:

$$\lambda_{\mathrm{c}} = -\frac{\int_0^c \left[h_{11}(x',c,\theta)\sigma_{y'y'}(x') + h_{12}(x',c,\theta)\sigma_{x'y'}(x') \right] \mathrm{d}x'}{\int_0^c h_{11}(x',c,\theta)\sigma_{y'y'}(x')\mathrm{d}x'} = -1 - \frac{\int_0^c h_{12}(x',c,\theta)\sigma_{x'y'}(x')\mathrm{d}x'}{\int_0^c h_{11}(x',c,\theta)\sigma_{y'y'}(x')\mathrm{d}x'} \tag{11}$$

Finally, K'_{II} obtained with the second of Eqs. 10, introducing the λ_{c} value calculated with Eq. 11, is the estimated value of K_{II}, according to the proposed assumption.

4 Model validation

A parametric FE model was developed for the validation analysis. The quarter point numerical technique was used with the software ANSYS [32]. Contact elements (frictionless) were placed at the crack faces, in order to

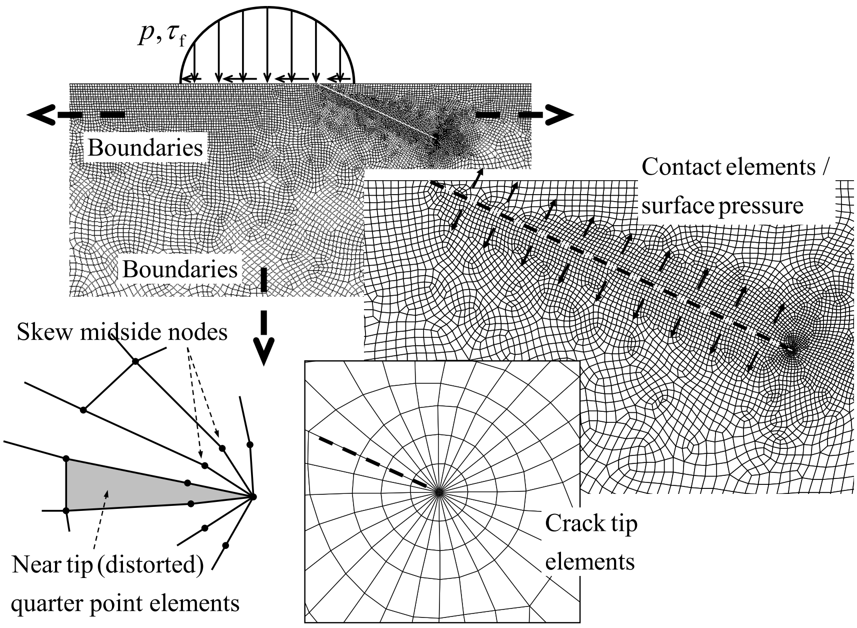

Figure 7: FE model to calculate the SIFs with the quarter point technique.

model both separation (with pressurization) and crack closure, Fig. 7. A convergence analysis was performed to verify that an accurate result can be obtained with 100 elements along the crack faces, and a comparable element size in the crack region and in the high stress contact region, Fig. 7.

The proposed WF calculation, and the assumption to estimate K_{II} when the crack is closed, were validated both with the FE model and by comparing the results from the literature. Several analyses with different contact parameters are available in the literature. Two case studies were considered: the negative S/R analysis reported by Bower [11], where the crack experiences strong pressurization, Fig. 8, and a null friction analysis reported by Datsyshyn and Marchenko [10], where pressurization is inactive and the crack remains closed, Fig. 9. The data from these two studies were compared with the results obtained with the FE model and with the results obtained with the proposed WF calculation. The SIFs are reported as dimensionless quantities. In the literature, two definitions can be found for dimensionless SIFs: $F_{\mathrm{I(II)}} = K_{\mathrm{I(II)}}/(p_0\sqrt{\pi a})$ and $F_{\mathrm{I(II)}} = K_{\mathrm{I(II)}}/(p_0\sqrt{a})$. In this paper the definitions: $F_{\mathrm{I}} = K_{\mathrm{I}}/(p_0\sqrt{\pi a})$, $F_{\mathrm{II}} = K_{\mathrm{II}}/(p_0\sqrt{\pi a})$ are used. The position of the center of the contact x_{c} is also given in a dimensionless form by adopting the half–width of the contact a as a normalizing quantity, as a consequence, the contact pressure is over the crack mouth when $-1 \leq x_{\mathrm{c}}/a \leq 1$.

The WF predictions almost perfectly match the references in the first part of Fig. 8 when the pressurization is active. The relative difference is in the order of 1%. This result was obtained with an appropriate discretization, which was then applied for all the other calculations. The Hertz half–width was divided into 200 uniformly loaded cells (Fig. 6(a) shows a coarser discretization for graphical purposes only). The sequence of the contact center position required from 100 to 200 divisions depending on the SIF trends, for example Fig. 8 shows very steep derivatives at the beginning of the pressurization. Finally, the crack length WF was divided into 100 divisions for an accurate numerical integration. Pressurization caused a high mode I SIF maximum value. The mode II SIF also experienced high values because of the coupling effect. In the final part of the contact transit the crack is closed, because the pressurization reduces its intensity and the Hertz pressure closure effect is predominant. Here K_{I} is zero, and the crack is only loaded by K_{II}. Bower performed a stick & slip analysis [11], while the present calculation was limited to the frictionless contact between the crack faces. Similarly the crack face contact was modeled as frictionless in the FE model, as mentioned above, and an excellent comparative result between the FE and WF models was found as reported in Fig. 8(a). The relative difference

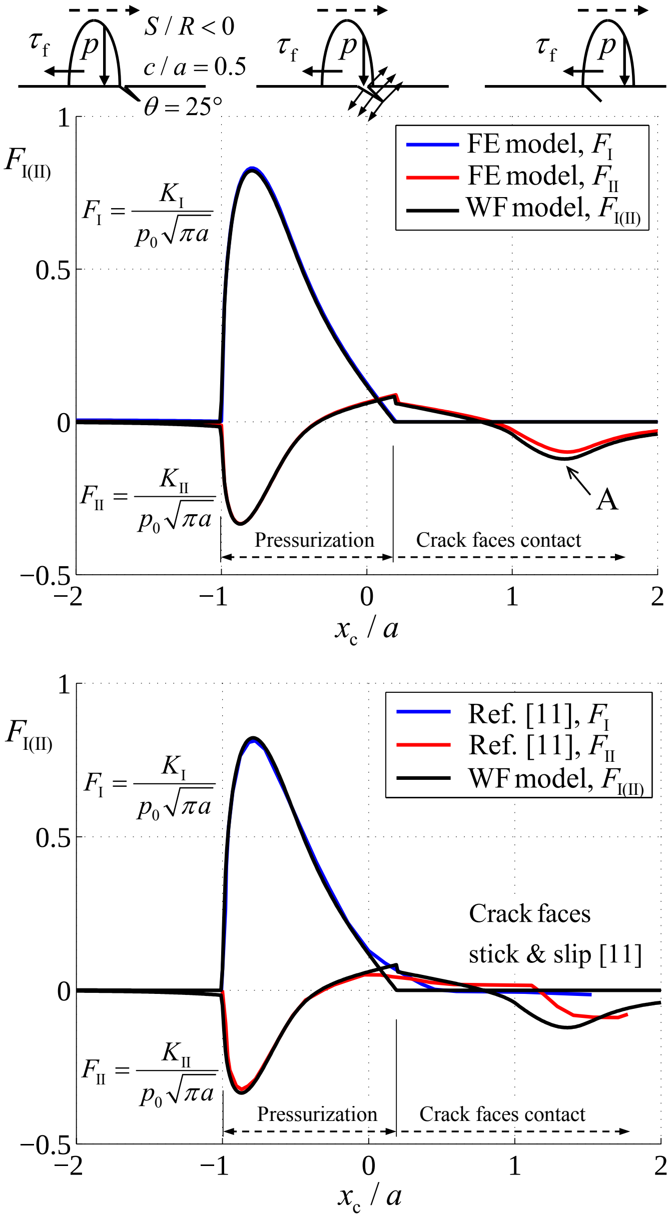

(a)

(b)

Figure 8: Validation of the proposed WF calculation, with the FE model and the literature data. (a) Negative S/R, $f = 0.05$, $\theta = 25°$, $c/a = 0.5$. (b) Null friction, $\theta = 150°$, $c/a = 1$.

of the proposed model and the trends obtained by Bower in the final part of the contact transit is small compared to the maximum dimensionless mode I and mode II stress intensity factor values.

The crack remains closed during the entire contact transit of the second analysis, Fig. 9. When the crack closes, the WF prediction of K_{II} is affected by a slightly higher error, due to the assumption for finding the distribution of crack face contact pressure $p_c(x')$. This inaccuracy is highest for the extreme K_{II} values. Figure 10 shows the three situations referred to as A, B, C in Figs. 8, 9. For all the three configurations the contact pressure between the crack faces $p_c(x')$ is shown, obtained both by the FE analysis and with the assumption of proportionality with the nominal normal stress distribution, as previously described.

These three configurations show quite different contact pressure distributions. With the contact condition A in

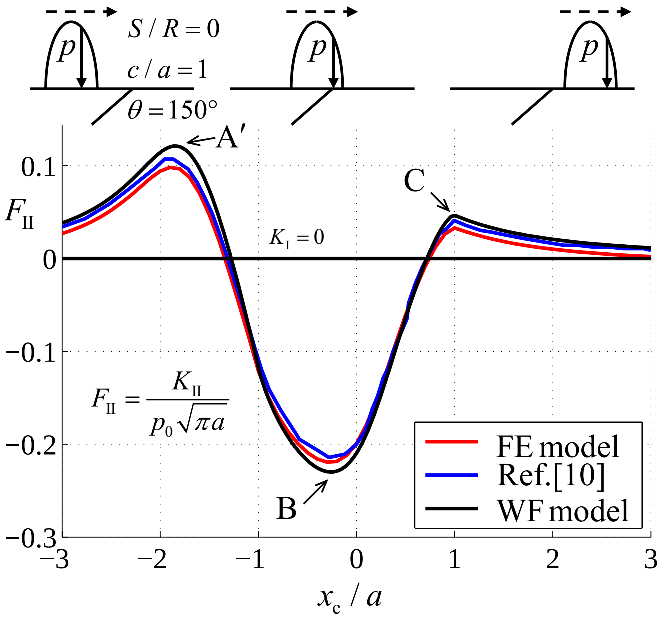

Figure 9: Validation of the proposed WF calculation, with FE model and literature data. (a) Negative S/R, $f = 0.05$, $\theta = 25°$, $c/a = 0.5$. (b) Null friction, $\theta = 150°$, $c/a = 1$.

Fig. 8, similar to the contact condition A′ in Fig. 9, the Hertz load is away from the crack but its projection is still over the crack tip. The crack is partially open, as shown by the FE simulation, indeed the contact pressure between the crack faces is zero near the surface. Although the partially open crack was not considered, in the present WF model, the nominal stress was found to be low in the initial part of the crack in agreement with the partially open crack. With configuration B, on the other hand, the Hertz load is entirely over the crack, the normal stress distribution does not show steep gradients, and thus the $p_c(x')$ proposed in the WF model is very similar to the FE $p_c(x')$, consequently the relative discrepancy of K_{II} is smaller. Finally, configuration C shows a contact distribution at the border of the crack mouth, while the crack is in the opposite direction. The loose contact is at the end of the crack line, thus *internally* the crack is partially open. In this configuration too, the assumption proposed produces an acceptable result, both in terms of the crack contact distribution and the mode II SIF. All the investigated configurations showed that the dimensionless factor is near unity $\lambda_c \approx -1$, as suggested by Eq. 11. The crack face contact pressure is approximately equal to the compressive nominal stress itself, however the proposed correction led to greater accuracy.

5 Applications

5.1 Parametric analysis

The proposed WF calculation algorithm was used to evaluate different contact conditions and parametric analyses were performed. A negative S/R was considered, where the dominating effect was the mode I SIF which underwent a positive cycle because of the pressurization. The dependencies investigated were coefficient of friction, surface angle and size of the crack. A weak dependency of both the SIF trends was found in terms of the friction coefficient f, relating the shear traction τ_f to the Hertz contact pressure p, in the wide range $f = 0.01 - 0.2$, Fig. 11. A strong dependency, on the other hand, was found in terms of the crack angle θ, Fig. 12. The shallower the crack, the higher the extreme values of the SIFs. The effect of the angle was more pronounced for small values. The SIF ranges approximately doubled when the θ angle was reduced from 30°

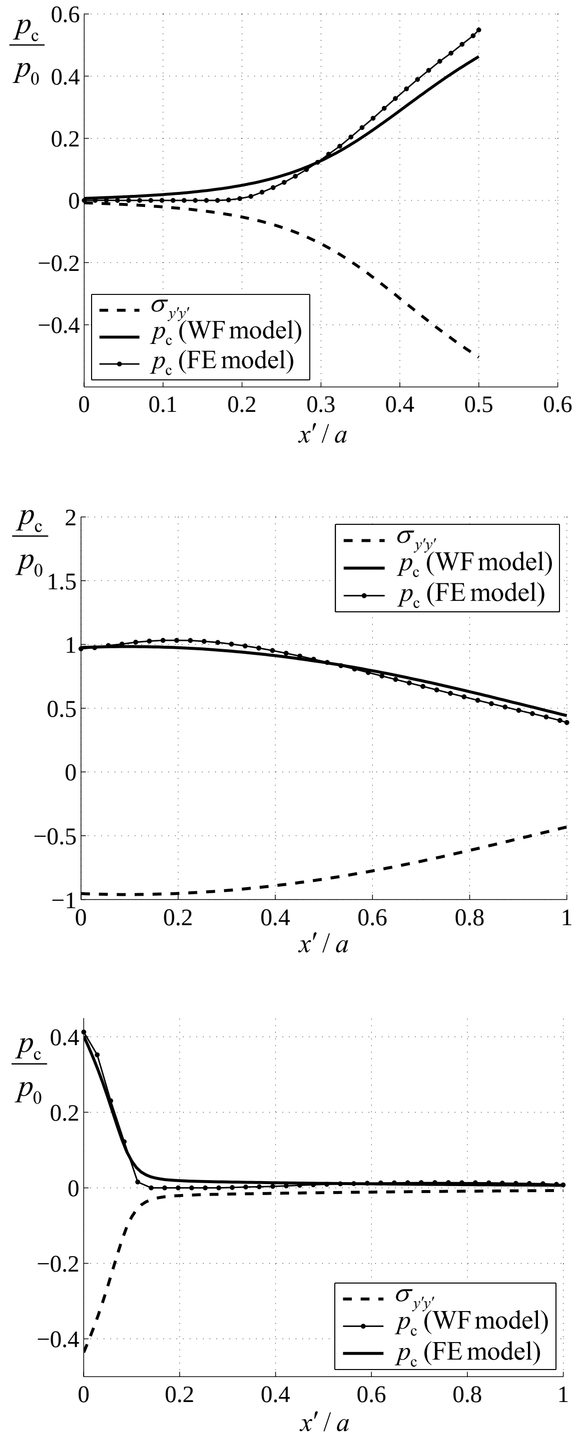

(a)

(b)

(c)

Figure 10: Comparison of crack faces contact distribution: (a) configuration A of Fig. 8, (b) configuration B of Fig. 9, (c) configuration C of Fig. 9.

to 15°, while they changed slightly for $\theta > 30°$.
Finally, the effect of the crack size was also investigated. Obviously, the larger the crack, the higher the values of K_{I} and K_{II}, Fig. 13. Figure 14 shows that this dependency is almost linear for different surface angles.

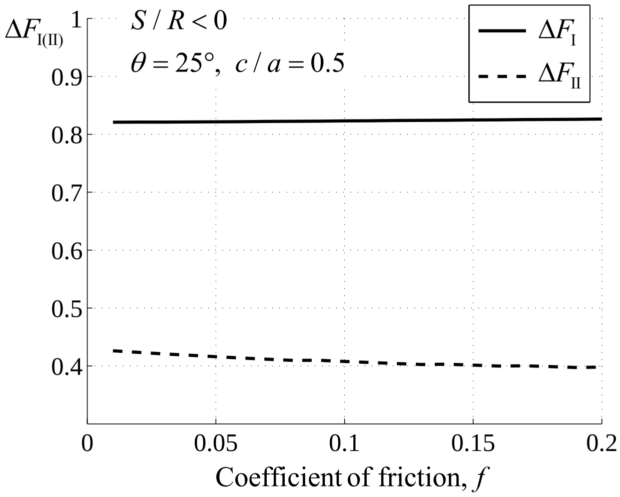

Figure 11: Dependency of dimensionless SIF ranges $\Delta F_{\mathrm{I}}, \Delta F_{\mathrm{II}}$ on the coefficient of friction f.

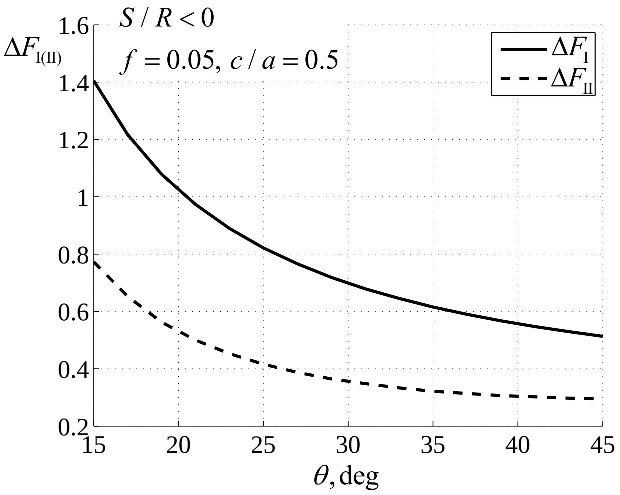

Figure 12: SIF ranges dependency with the crack angle.

5.2 Residual stresses

As mentioned above, the residual stress can be efficiently taken into account within the proposed WF calculation. The small and shallow cracks are mainly important for the fatigue surface pitting problem, thus near surface uniform residual stress was considered, even though the proposed procedure can elaborate any residual stress distribution along the depth. The residual stress at the surface, or slightly below the surface, is biaxial. Moreovoer, the transversal component (perpendicular to the plane of the problem) does not influence the SIFs, as mentioned above. Residual stress can therefore be defined here by a unique scalar value σ_{RS}, which can be reported as a dimensionless ratio with the maximum contact pressure p_0. Different residual stress levels were considered: $\sigma_{\mathrm{RS}}/p_0 = -1, 0.5, 0, 0.5$ (negative σ_{RS}/p_0 means compressive residual stress). The opening of the crack is reduced by compressive residual stress, while it is increased by tensile residual stress. A tensile residual stress produces a higher K_{I} maximum value, and a delayed crack closure after pressurization. A tensile residual stress also causes a *positive* K_{I} while the Hertz distribution is away from the crack, and a reopening after the crack has closed. The residual stresses also shift the value of K_{II}, which is not zero when

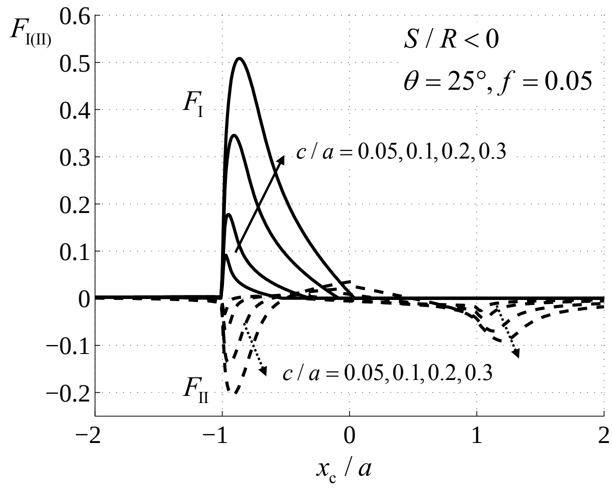

Figure 13: Dimensionless K_{I} and K_{II} trends for different crack sizes.

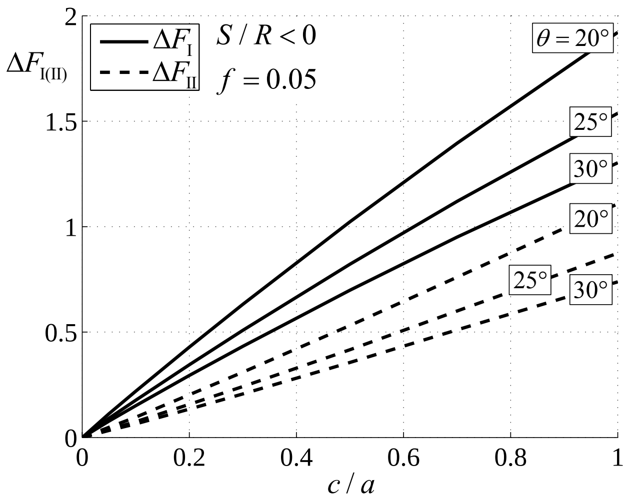

Figure 14: Linear dependency of SIF ranges with the crack size, higher SIF ranges for shallower cracks.

the Hertz distribution is not near the crack, Fig. 15. The closure of the compressive stress has a different effect depending on the size of the crack. Smaller cracks are more intensively affected. When small and with a highly compressive residual stress state, the crack may even remain closed, Fig. 16.

6 Conclusions

The weight function technique was used to calculate stress intensity factors for inclined surface cracks loaded by traveling Hertz pressure and proportional friction. Any different surface pressure and shear traction can be modeled, even if such tractions vary during transit. For example involute gear tooth loading, especially with profile modification, can show curvature changes during contact transit and pressure variation because of teeth load sharing. Surface pressure and shear traction were modeled as uniformly loaded cell distributions in order to accurately find the stresses below the surface. The effect of pressurization and residual stresses were also modeled, by including these terms in the weight function integrals. High accuracy was obtained simply by reducing the size of each uniformly loaded cell and by introducing a proper discretization of the crack

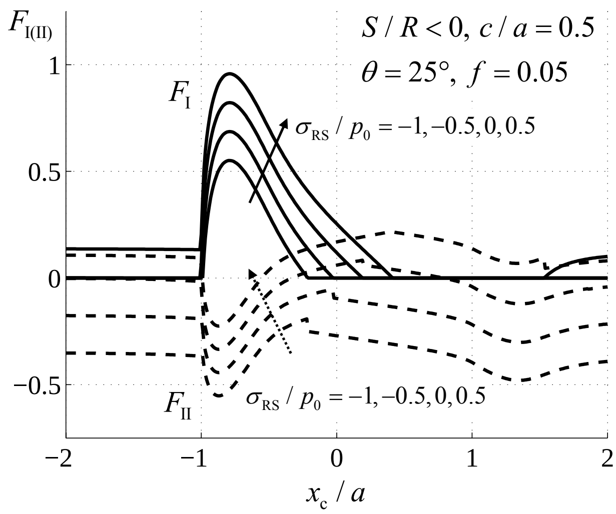

Figure 15: Dimensionless K_{I} and K_{II} trends for different residual stress intensities.

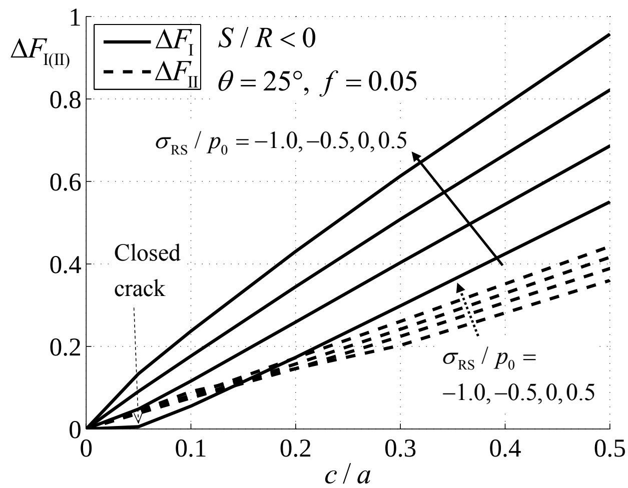

Figure 16: Crack size dependency of SIF ranges with different residual stress intensities.

line where a numerical integration of the weight function was performed. The high efficiency of the weight function calculation involved very little computational time despite the high level of discretization required.

The proposed model was successfully verified on the basis of available data in the literature and also with a dedicated finite element model. Very accurate comparative results were obtained during pressurization, which produced a positive mode I stress intensity factor. In order to find the mode II stress intensity factor, when the crack is closed, it was assumed that the contact pressure distribution at the crack face was proportional to nominal stress. This hypothesis was then verified on several geometry configurations.

Parametric analyses were performed for different pressurization and results discussed. The friction coefficient was almost non influential, while the angle of the crack was very effective, especially for small values. The stress intensity factor ranges were found to be depend almost linearly on the crack size. The effects of the residual stress were also parametrically investigated. As expected, a compressive residual stress produced a smaller pressurization mode I and earlier crack closure. This effect was stronger for smaller cracks. The compressive residual stress was able to overcome the pressurization and even keep the crack closed.

This analysis can provide important information about any surface treatment designed to improve fatigue strength. It thus extends the optimization of the surface treatment depth [33] to the field of rolling contact fatigue where the mode I loading is generated by pressurization rather than any external load.
An evolution of the proposed study would be to introduce the weight function for the surface kinked crack. This was recently proposed in Ref. [34] and it could be used in order to find the stress intensity factors of the pitting crack after a first orientation deviation, while in this study the crack was limited to the simple straight crack configuration.

Acknowledgments

AVIO Propulsione Aerospaziale S.p.A. is acknowledged for supporting the research published in this paper.

References

[1] D.P. Townsend. *Dudley's Gear Handbook*. McGraw–Hill, 2nd edition, 1991.

[2] T.E. Tallian. *Failure Atlas for Hertz Contact Machine Elements*. ASME Press, 1992.

[3] G. Fajdiga, S. Glodež, and J. Kramar. Pitting formation due to surface and subsurface initiated fatigue crack growth in contacting mechanical elements. *Wear*, 262(9–10):1217–1224, 2007. DOI: 10.1016/j.wear.2006.11.016.

[4] S. Glodež. A new model for the numerical determination of pitting resistance of gear teeth flanks. *Fatigue & Fracture of Engineering Materials & Structures*, 20(1):71–83, 1997. DOI: 10.1111/j.1460-2695.1997.tb00403.x.

[5] D. Nélias, M.L. Dumont, F. Champiot, A. Vincent, and D. Girodin. Role of Inclusions, Surface Roughness and Operating Conditions on Rolling Contact Fatigue. *Journal of Tribology, ASME*, 121(2):240–251, 1999. DOI: 10.1115/1.2833927.

[6] D. Nélias, M.L. Dumont, F. Couhier, G. Dudragne, and L. Flamand. Experimental and Theoretical Investigation on Rolling Contact Fatigue of 52100 and M50 Steels Under EHL or Micro-EHL Conditions. *Journal of Tribology, ASME*, 120(2):184–200, 1998. DOI: 10.1115/1.2834407.

[7] A.V. Olver, L.K. Tiew, S. Medina, and J.W. Choo. Direct observations of a micropit in an elastohydrodynamic contact. *Wear*, 256(1–2):168–175, 2004. DOI: 10.1016/S0043-1648(03)00374-0.

[8] A.V. Olver. The mechanism of rolling contact fatigue: an update. *Proceedings of the Institution of Mechanical Engineers, Part J: Journal of Engineering Tribology*, 219(5):313–330, 2005. DOI: 10.1243/135065005X9808.

[9] S. Way. Pitting due to rolling contact. *Journal of Applied Mechanics, ASME*, 57:A49–A58, 1935.

[10] O.P. Datsyshyn and H.P. Marchenko. Stressed state of a half plane with shallow edge crack under hertzian loading (a survey). *Materials Science*, 44(1):22–34, 2008. DOI: 10.1007/s11003-008-9039-5.

[11] A.F. Bower. The Influence of Crack Face Friction and Trapped Fluid on Surface Initiated Rolling Contact Fatigue Cracks. *Journal of Tribology, ASME*, 110(4):704–711, 1988. DOI: 10.1115/1.3261717.

[12] L.M. Keer and M.D. Bryant. A pitting model for rolling contact fatigue. *Journal of Lubrication Technology, ASME*, 105:198–205, 1983.

[13] K.L. Johnson. The strength of surfaces in rolling contact. In Journal of Mechanical Engineering Science, editor, *Proceedings of the Institution of Mechanical Engineers*, volume 203, pages 151–163, 1989.

[14] X. Jin, L.M. Keer, and E.L. Chez. Numerical simulation of growth pattern of a fluid–filled subsurface crack under moving hertzian loading. *International Journal of Fracture*, 142(3–4):219–232, 2006. DOI: 10.1007/s10704-006-9026-5.

[15] Y. Murakami, C. Sakae, K. Ichimaru, and T. Morita. Experimental and Fracture Mechanics Study of the Pit Formation Mechanism Under Repeated Lubricated Rolling-Sliding Contact: Effects of Reversal of Rotation and Change of the Driving Roller. *Journal of Tribology, ASME*, 119(4):788–796, 1997. DOI: 10.1115/1.2833886.

[16] G. Fajdiga and M. Sraml. Fatigue crack initiation and propagation under cyclic contact loading. *Engineering Fracture Mechanics*, 76(9):1320–1335, 2009. DOI: 10.1016/j.engfracmech.2009.02.005.

[17] S. Glodež, Z. Ren, and G. Fajdiga. Computational modelling of the surface fatigue crack growth on gear teeth flanks. *Communications in Numerical Methods in Engineering*, 17(8):529–541, 2001. DOI: 10.1002/cnm.427.

[18] Z. Ren, S. Glodež, G. Fajdiga, and M. Ulbin. Surface initiated crack growth simulation in moving lubricated contact. *Theoretical and Applied Fracture Mechanics*, 38(2):141–149, 2002. DOI: 10.1016/S0167-8442(02)00091-5.

[19] J.W. Ringsberg and A. Bergkvist. On propagation of short rolling contact fatigue cracks. *Fatigue & Fracture of Engineering Materials & Structures*, 26(10):969–983, 2003. DOI: 10.1046/j.1460-2695.2003.00657.x.

[20] M. Beghini, L. Bertini, and V. Fontanari. Weight function for an inclined edge crack in a semiplane. *International Journal of Fracture*, 99(4):281–292, 1999. DOI: 10.1023/A:1018791622562.

[21] M. Beghini, L. Bertini, and V. Fontanari. Stress intensity factors for an inclined edge crack in a semiplane. *Engineering Fracture Mechanics*, 62(6):607–613, 1999. DOI: 10.1016/S0013-7944(99)00011-9.

[22] M. Beghini, L. Bertini, and V. Fontanari. A weight function technique for partially closed inclined edge cracks analysis. *International Journal of Fracture*, 112(1):57–68, 2001. DOI: 10.1023/A:1013529608424.

[23] M. Beghini, L. Bertini, and V. Fontanari. A weight function for 2D subsurface cracks under general loading conditions. *Engineering Fracture Mechanics*, 75(3–4):427–439, 2008. DOI: 10.1016/j.engfracmech.2007.02.017.

[24] C. Santus, M. Beghini, I. Bartilotta, and M. Facchini. Surface and subsurface rolling contact fatigue characteristic depths and proposal of stress indexes. *International Journal of Fatigue*, 45:71–81, 2012. DOI: 10.1016/j.ijfatigue.2012.06.012.

[25] G. Stachowiak and A.W. Batchelor. *Engineering Tribology*. Butterworth–Heinemann, 2nd edition, 2000.

[26] Y. Ding and N.F. Rieger. Spalling formation mechanism for gears. *Wear*, 254(12):1307–1317, 2003. DOI: 10.1016/S0043-1648(03)00126-1.

[27] M. Boniardi, F. D'Errico, and C. Tagliabue. Influence of carburizing and nitriding on failure of gears – A case study. *Engineering Failure Analysis*, 13(3):312–339, 2006. DOI: 10.1016/j.engfailanal.2005.02.021.

[28] T.L. Anderson. *Fracture Mechanics: Fundamentals and Applications*. CRC Press, 3rd edition, 2005.

[29] K.L. Johnson. *Contact Mechanics*. Cambridge University Press, 1987.

[30] E. Ciulli. Tribology research trends in Italy. *Proceedings of the Institution of Mechanical Engineers, Part J: Journal of Engineering Tribology*, 223(8):1091–1113, 2009. DOI: 10.1243/13506501JET543.

[31] M. Beghini and C. Santus. Analysis of the plane contact with discontinuous curvature. *Meccanica*, 42(1):95–106, 2007. DOI: 10.1007/s11012-006-9025-7.

[32] E. Madenci and I. Guven. *The Finite Element Method and Applications in Engineering Using ANSYS®*. Springer, 2006.

[33] M. Benedetti, V. Fontanari, C. Santus, and M. Bandini. Notch fatigue behaviour of shot peened high-strength aluminium alloys: Experiments and predictions using a critical distance method. *International Journal of Fatigue*, 32(10):1600–1611, 2010. DOI: 10.1016/j.ijfatigue.2010.02.012.

[34] M. Beghini, M. Benedetti, V. Fontanari, and B.D. Monelli. Stress intensity factors of inclined kinked edge cracks: A simplified approach. *Engineering Fracture Mechanics*, 81:120–129, 2012. DOI: 10.1016/j.engfracmech.2011.11.005.